Imaging the Electron-Phonon Interaction at the Atomic Scale

Igor Altfeder,[1,*] K. A. Matveev,[2] and A. A. Voevodin[1]

[1]*Nanoelectronic Materials Branch, Air Force Research Laboratory, Wright Patterson AFB, Ohio 45433, USA*
[2]*Materials Science Division, Argonne National Laboratory, Argonne, Illinois 60439, USA*

(Received 22 June 2012; published 16 October 2012)

Thin Pb films epitaxially grown on 7×7 reconstructed Si(111) represent an ideal model system for studying the electron-phonon interaction at the metal-insulator interface. For this system, using a combination of scanning tunneling microscopy and inelastic electron tunneling spectroscopy, we performed direct real-space imaging of the electron-phonon coupling parameter. We found that λ increases when the electron scattering at the Pb/Si(111) interface is diffuse and decreases when the electron scattering is specular. We show that the effect is driven by transverse redistribution of the electron density inside a quantum well.

DOI: 10.1103/PhysRevLett.109.166402 PACS numbers: 71.38.−k, 68.37.Ef, 73.21.Fg

The electron-phonon interaction plays a crucial role in (a) formation of charge density waves in low-dimensional conductors [1], (b) superconductivity in metals [2], (c) electronic growth of magic-sized films [3–6] and quantum dots [7,8], and (d) thermal transport across metal-insulator interfaces [9]. Study of the electron-phonon coupling at subnanometer and atomic length scales is important for a basic understanding of interactions and energy transport in nanostructures and for development of materials with enhanced thermal characteristics. As we shall show in this Letter, such a study can be performed using a combination of scanning tunneling microscopy (STM) and inelastic electron tunneling spectroscopy [10–16] (IETS). The STM-IETS combination represents a powerful technique for the study of molecular vibrational spectra [12–15], surface phonon density of states [16], and inelastic Friedel oscillations [11]. The most developed STM-IETS imaging mode is spatial mapping of a frequency domain: distinguishing local vibrations of adsorbed molecules from native substrate vibrations [12–15] or distinguishing the phonon density of states for differently structured surface regions [16].

In this Letter, we show for the first time that the spatial distribution of the electron-phonon interaction (EPI) parameter λ can be directly visualized using STM. A perfect model system for experimental realization of an alternative imaging mode of the STM-IETS technique, spatial mapping of a λ domain, is a thin Pb film epitaxially grown on 7×7 reconstructed Si(111). The top surfaces of these films represent atomically flat (111)-oriented crystal planes free of defects and stacking faults, whose vibrational spectra are essentially determined by the Debye frequency of Pb. On the other hand, the coupling strength of these vibrations with electron waves confined inside Pb films can be strongly affected by the quantum size effect (QSE) and the electron scattering at interfaces. Assuming *ballistic* reflection of electrons at surfaces, the electronic wave functions inside a quantum well (QW) represent the superposition of incident and specular reflected waves, whereas the allowed electronic states can be determined from the quantum mechanical phase accumulation rule:

$$2k_{\perp}H = 2\pi n, \tag{1}$$

where $k_{\perp}$ is the transverse component of the electron's wave vector and H is film thickness. As a consequence of ballistic reflections and interference, the electron density inside a thin film redistributes and becomes strongly modulated along the thickness direction. Such a redistribution of the electron density (see Fig. 1, curve 1) becomes especially dominant in the ultrathin film limit and is capable of modifying the electron-phonon interaction parameter λ with respect to its bulk value: it is well known that EPI depends

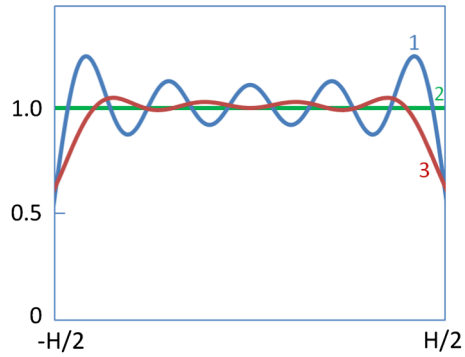

FIG. 1 (color online). A significant density redistribution occurs in QW when surface electron scattering changes from ballistic to diffuse. On curve 1, five interference maxima correspond to five occupied QW states. For Pb films, this corresponds to a thickness of $H = 10a$ (atomic layers). When surface scattering is diffuse, the interference maxima become suppressed. The density distribution flattens and approaches a constant bulk value corresponding to curve 2. For surface roughness $\sim a$, diffuse scattering strongly affects short-wavelength QW modes (closest to the Fermi level) and weakly affects long-wavelength modes. The resulting density distribution is shown on curve 3.

on the electron density distribution [17]. For example, the earlier study of the temperature dependent QW linewidth in thin Pb films has shown a gradually decreasing trend for λ with decreasing film thickness [18], superimposed with two-monolayer-period oscillations [19]. In principle, the interference-induced electron density distribution can be modified or suppressed if *diffuse* scattering occurs at the film surface, as we also show in Fig. 1. This behavior is very similar to what occurs in optics: interference in the Fabry-Perot geometry only develops when both surfaces are smooth and do not produce a diffuse scattering of waves. In thin epitaxial metal films, the electronic QSE becomes suppressed if diffuse scattering occurs at the film-substrate interface due to defects or lattice mismatch. Remarkably, a clear transition between these two opposite limits (ballistic reflection vs diffuse scattering) can be directly observed in the Pb/Si(111)7×7 system [20]. It has been shown that corner holes and dimer dislocations of the buried 7×7 interface cause local suppression of electron interference along the thickness direction of the film [20]. These interfacial scattering centers are of atomic size (a), whereas the Fermi wavelength in Pb is very close to $4a$. Because of this effect, the structure of the Pb/Si(111)7×7 interface can be directly visualized by STM when the tunneling bias is close to the energy of the electronic QW resonance [20]. It has been shown that high lateral resolution of the interface is related to Fermi surface nesting [21], focusing electrons in these films along the crystal directions [111], i.e., in the direction normal to the film boundary. Thus, by monitoring simultaneously (a) the structure of the Pb/Si(111) interface on constant-current STM topographic images and (b) the spatial distribution of the IETS peak heights, one can experimentally establish the connection between the type of electron scattering at the interface and the strength of electron-phonon interaction in thin film. Because it was shown by theory [22] that the height of the IETS resonant peaks scales as λ^2, such simultaneous STM and IETS imaging could reveal the connection between local λ^2 and the atomic structure of the interface [23].

The experiments were performed in a dual-chamber ultrahigh vacuum (UHV) system, with base pressure 5×10^{-11} Torr, equipped with variable temperature STM operating at 25 K, an ion gun for surface cleaning, and a thermal evaporator for *in situ* deposition of Pb atoms. Before deposition, the Si(111) surface was cleaned by a sequence of 1100 °C UHV annealing and Ne^+ ion sputtering. This procedure was repeated until the clean 7×7 reconstructed surface of Si(111) was observed by STM. After cleaning, Pb atoms were deposited onto this surface at a rate of 0.1 monolayers (ML) per minute. During deposition, the substrate was kept at room temperature. Previous studies have shown that such a deposition procedure yields atomically flat Pb islands with growth plane (111), and the 7×7 reconstruction of Si(111) remains preserved under these islands [20,24]. STM measurements were performed at 25 K, using a PtIr tip (from Bruker Corp.) which was annealed in UHV using the electron beam technique. For IETS measurements, we applied tunneling bias modulation at a frequency of 2.5 KHz with 4 mV amplitude, and we detected the second harmonic of this modulation in the tunneling current using a lock-in amplifier in order to determine $\partial^2 I/\partial V^2$. As it was suggested earlier [25], with variable temperature STM, the IETS peak height may additionally increase due to the lowering of the tip apex temperature and the narrowing of its Fermi distribution for surface regions with higher EPI. Because of this reason, the λ dependence of the IETS peaks may be even stronger than theory predicted λ^2.

In Fig. 2, we show the large scale, 0.95×0.95 μm^2 STM image of the studied sample. The lateral sizes of room temperature grown Pb islands can be as large as 0.5 μm, whereas their height distribution peaks at 9 ML. The energies of transverse QW resonances in Pb islands, E_n, can be found from the bulk dispersion relation $E(k_\perp)$, with $k_\perp$ determined by Eq. (1). Electronic density of states spectra of such islands have been reported in a large number of publications, and their QW resonant energies for different numbers of Pb layers are well established using various experimental techniques [26–29]. In particular, for 9 ML height islands, the highest occupied and the lowest unoccupied QW resonances are located at 500 meV below and 600 meV above the Fermi level, respectively, and are separated by a 1.1 eV spectral gap. In the inset of Fig. 3, we show the tunneling I-V characteristic of the 9 ML Pb island in our sample.

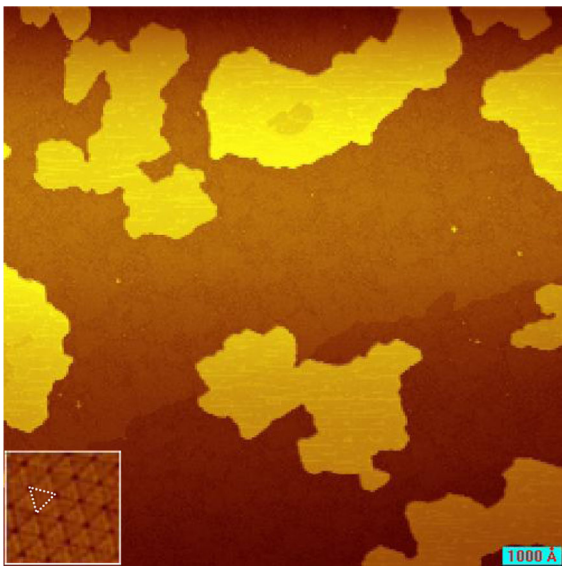

FIG. 2 (color online). The 0.95×0.95 μm^2 STM image of the studied sample. Atomically flat Pb islands were *in situ* deposited on the Si(111) surface at room temperature. The image was acquired at a tunneling current of 0.5 nA and a tunnel bias of 500 mV. Inset: 120×120 Å^2 STM image of the 7×7 reconstructed Si(111) before Pb deposition.

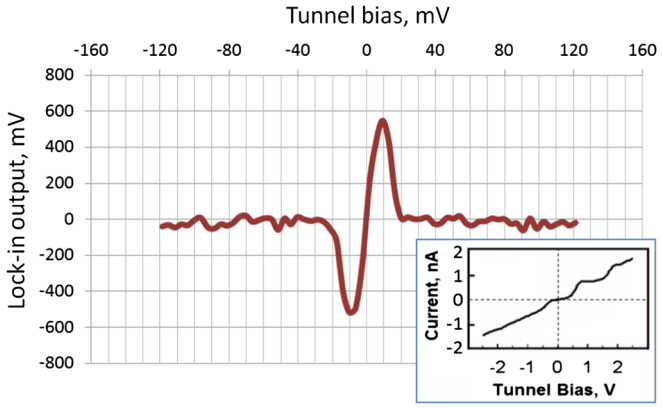

FIG. 3 (color online). The inelastic electron tunneling spectrum measured on top of the 9 ML Pb island. Resonant phonon emission peaks develop at a ±9 mV tunnel bias. Inset: tunnel I-V curve for the same island measured in a broader bias range. Steps on this curve are due to QW resonances from transverse electron interference. The decrease of the barrier height at large bias [26] was compensated by a slow increase of a tunneling gap, at a rate of 0.4 Å per $|V|$.

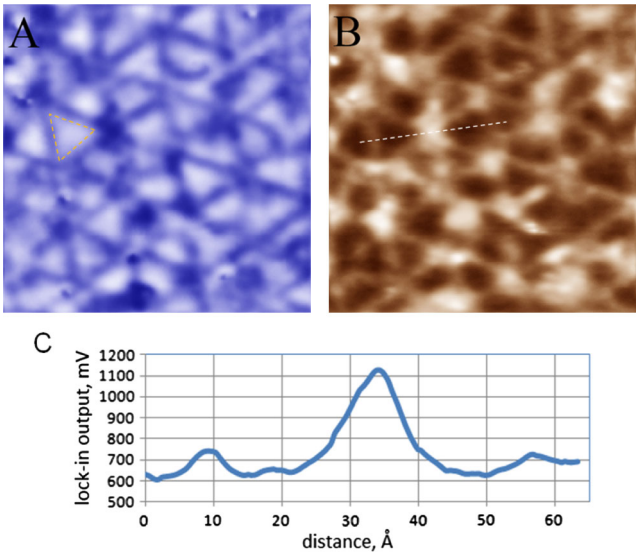

FIG. 4 (color online). (a),(b) 120×120 Å^2 STM and IETS maps simultaneously, line-by-line, acquired on the surface of the 9 ML Pb island at a 1 nA tunneling current. The STM image (a) was obtained at a tunnel bias of 750 mV. The IETS image (b) was acquired at a tunnel bias of 9 mV. The dashed line in (a) illustrates an electronic image of a triangular domain shown earlier in the inset of Fig. 2. (c) Cross section of the IETS image in (b).

In Fig. 3, we show the IETS spectrum recorded on top of the 9 ML height Pb island. We observe a symmetric pair of phonon emission peaks at a tunnel bias of ±9 mV. The energy of these phonons is close to the Debye temperature of Pb ($\theta_D = 100$ K). These are zone-edge Pb phonons [30], with a density of states peak arising from the diverging $\partial k/\partial\omega$. Because of the large time required for measurements of the IETS signals (and thermal drift, which occurs during this time), the curve in Fig. 3 represents the phonon density of states for the 9 ML Pb island spatially averaged over a ~2 nm distance across the surface of the island. In order to reveal the spatial distribution of the IETS resonant peaks on the surface of the island, we performed simultaneous STM and IETS imaging. For this purpose, *each* scan line was repeated twice: (a) the first time at a 750 mV tunnel bias to record the spatial distribution of the electron-interference signal on topographic STM images and (b) a second time at a 9 mV tunnel bias to record the spatial distribution of the IETS peak. These simultaneously acquired 120×120 Å^2 images are shown in Fig. 4. The STM image on Fig. 4(a) shows the triangular domains of the buried Pb/Si(111) interface, with a lateral period of 28 Å, separated from each other by dimer dislocations whose intersections are the corner holes of the 7×7 structure. The bright triangular domains in Fig. 4(a) represent interfacial regions characterized by ballistic (specular) electron reflection. Inside these regions, strong transverse electron interference takes place. The interference effect is further magnified because the electron group velocity is directed along the [111] crystal axis, normally to the film boundary. Because of this, the electron density of states exhibits a strong interference peak at 600 mV, accompanied by a steplike increase of a tunneling current, as shown in the inset of Fig. 3. In the constant-current STM imaging mode, this interference signal is manifested as a ~0.5–1.0 Å increase of the effective height of the island. As one can see in Fig. 4(a), such an interference signal is lower (or entirely absent) on top of interfacial defects where electron scattering acquires a diffuse component and the QSE becomes locally suppressed. On a simultaneously measured IETS map, shown in Fig. 4(b), we can also see the triangular domains, and we observe the increase of the phonon emission peak in the defected regions of the interface. Essentially, Fig. 4(b) shows an intersecting network of ''virtual nanowires'' with enhanced electron-phonon coupling that develops inside Pb islands. To characterize the increase of the IETS signal quantitatively, in Fig. 4(c) we show the cross section of an IETS image. From this cross section, we find that the IETS peak increases by 25% on top of the dimer dislocations and nearly doubles on top of the corner holes. Since both images in Fig. 4 have been acquired in the constant-current regime of STM, the experimentally observed increase of the IETS peak height indeed shows the relative increase of the inelastic portion of the tunneling current with respect to the total tunneling current. Assuming theory predicted λ^2 dependence of the IETS peak heights, the corresponding increases of the electron-phonon interaction parameter λ can be estimated as 12% and 40%, respectively. We would like to stress here that the local increase of λ most likely occurs on top of its already reduced thin film value at

atomically flat regions of the Pb/Si(111) interface rather than with respect to its bulk value [18].

Our results show the previously unknown connection between the strength of the electron interference in thin films and the strength of the electron-phonon interaction. As we argued in the beginning of this Letter, this connection most likely has to do with the spatial redistribution of the electron density along the thickness direction of the film caused by a specular reflection of electron waves. Because the electron tunneling in our experiment occurs into QW states rather than into surface states, the process of phonon emission, in principle, may occur anywhere throughout the film thickness, not necessarily at its top surface. However, despite the fact that the total electron density, i.e., the density averaged along the film thickness, remains the same regardless of the type of interfacial scattering, the effective value of λ apparently does not average in the same manner: it decreases when the electron scattering is ballistic and increases when the electron scattering becomes diffuse. The physical reason for this will be explained below. The zone-edge 9 meV phonons that were studied in our experiment correspond to the L point of the face-centered-cubic Brillouin zone of Pb [30,31]. Their wave vector, $q = \pi/a$, is oriented along the crystal axis [111]. The characteristic wave vector of the interference-induced density oscillations ($Q \approx 2k_F$) is also oriented [111] and is very close to π/a. Therefore, a strong (nearly resonant) cross talk is anticipated between these phonons and the electrons confined inside Pb islands. The result of this cross talk, depending on the atomic-scale details of interaction, may be either (a) a strong enhancement or (b) a strong suppression of EPI under strong quantum confinement. As it was shown in the earlier study [18], λ gradually decreases with decreasing Pb thickness, suggesting that the second option (b) takes place: confinement-induced electron density oscillations cause a resonant suppression of λ [32]. This is why the elimination of the electron density oscillations due to the scattering on interfacial defects increases λ in our experiments.

Because the concept of diffuse scattering, which we referred to throughout this Letter, is frequently used in mesoscopic physics, but not so commonly for nanoscale systems, we will additionally clarify how exactly this concept works for the case of interfacial corner holes: scattering centers providing the strongest enhancement of λ. These are atomic-scale holes on the Si(111) surface arising from 7×7 reconstruction (see the inset of Fig. 2). On the initial stage of the Pb deposition, before the Stranski-Krastanov growth commences, these holes become filled with individual Pb atoms. The atomically flat quantum well, produced in this manner, contains a set of individual Pb adatoms attached to its bottom. These adatoms locally increase the film thickness by a and cause the accumulation of the additional interference path of $2a$, which for Pb corresponds to a half-wavelength or a 180°-phase shift. Because of the atomically small lateral size of these centers, the reflected waves, at these points of the interface, contain two 180°-shifted, with respect to each other, components cancelling each other and, thus, locally cancelling a specular reflection. As a result, electrons scatter at these regions of interface without $k_{||}$ conservation, i.e., diffusely. The only portion of transverse electron density oscillations, which is totally cancelled by this effect, corresponds to the highest occupied QW states: those closest to the Fermi level and therefore the most important for EPI [19]. This is illustrated by curve 3 in Fig. 1 [33]. The quarter-wavelength suppressors of specular reflection are now widely used for making antireflective coatings for the enhancement of optical lenses. We show that this approach also works on the atomic scale: not for the improved transmission of waves but for the improved transmission of heat because higher λ leads to the enhancement of interfacial heat conductance [9].

In conclusion, a new STM-based imaging technique, direct real-space imaging of the electron-phonon interaction parameter, was demonstrated using the combination of STM and IETS in thin metal films. The network of intersecting virtual nanowires with enhanced electron-phonon coupling was revealed using this technique inside thin Pb islands: the network whose superconducting properties may be quite different from the properties of bulk material. A surprising connection between the electron interference and the electron-phonon coupling parameter has been established. Because electrons represent dominant heat carriers in metals whereas phonons are the only heat carriers in insulators, the interfacial electron-phonon interaction plays a crucial role in the process of heat transport across metal-insulator interfaces. Our results suggest a novel approach for the nanoscale engineering of thermal interfaces with improved transport characteristics [34].

We want to acknowledge G. Levin, M. Hupalo, K. Walczak, V. Varshney, and A. Roy for interesting discussions. We also thank Dr. Joan Fuller, Program Manager of the AFOSR Thermal Sciences Program, for supporting our research.

*To whom all correspondence should be addressed.
Igor.Altfeder.Ctr@wpafb.af.mil

[1] T. M. Rice and G. K. Scott, Phys. Rev. Lett. **35**, 120 (1975).
[2] J. Bardeen, L. N. Cooper, and J. R. Schrieffer, Phys. Rev. **108**, 1175 (1957).
[3] Z. Zhang, Q. Niu, and C. K. Shih, Phys. Rev. Lett. **80**, 5381 (1998).
[4] M. Hupalo and M. C. Tringides, Phys. Rev. B **65**, 115406 (2002).
[5] J. Chen, M. Hupalo, M. Ji, C. Z. Wang, K. M. Ho, and M. C. Tringides, Phys. Rev. B **77**, 233302 (2008).
[6] S. H. Chang, W. B. Su, W. B. Jian, C. S. Chang, L. J. Chen, and T. T. Tsong, Phys. Rev. B **65**, 245401 (2002).

[7] G. Pawin, K. L. Wong, K. Y. Kwon, and L. Bartels, Science **313**, 961 (2006).
[8] I. B. Altfeder, J. J. Hu, A. A. Voevodin, and J. Krim, Phys. Rev. Lett. **102**, 136104 (2009).
[9] A. Majumdar and P. Reddy, Appl. Phys. Lett. **84**, 4768 (2004).
[10] J. Lambe and R. C. Jaklevic, Phys. Rev. **165**, 821 (1968).
[11] H. Gawronski, J. Fransson, and K. Morgenstern, Nano Lett. **11**, 2720 (2011).
[12] B. C. Stipe, M. A. Rezaei, and W. Ho, Science **280**, 1732 (1998).
[13] J. R. Hahn, H. J. Lee, and W. Ho, Phys. Rev. Lett. **85**, 1914 (2000).
[14] M. Grobis, K. H. Khoo, R. Yamachika, X. Lu, K. Nagaoka, S. G. Louie, M. F. Crommie, H. Kato, and H. Shinohara, Phys. Rev. Lett. **94**, 136802 (2005).
[15] L. Vitali, M. Burghard, M. A. Schneider, L. Liu, S. Y. Wu, C. S. Jayanthi, and K. Kern, Phys. Rev. Lett. **93**, 136103 (2004).
[16] H. Gawronski, M. Mehlhorn, and K. Morgenstern, Science **319**, 930 (2008).
[17] J. Bardeen and D. Pines, Phys. Rev. **99**, 1140 (1955).
[18] Y.-F. Zhang, J.-F. Jia, T.-Z. Han, Z. Tang, Q.-T. Shen, Y. Guo, Z. Q. Qiu, and Q.-K. Xue, Phys. Rev. Lett. **95**, 096802 (2005).
[19] C. Brun, I.-P. Hong, F. Patthey, I. Yu. Sklyadneva, R. Heid, P. M. Echenique, K. P. Bohnen, E. V. Chulkov, and W.-D. Schneider, Phys. Rev. Lett. **102**, 207002 (2009).
[20] I. B. Altfeder, D. M. Chen, and K. A. Matveev, Phys. Rev. Lett. **80**, 4895 (1998).
[21] J. R. Anderson and A. V. Gold, Phys. Rev. **139**, A1459 (1965).
[22] K. Walczak, Chem. Phys. **333**, 63 (2007).
[23] In order to experimentally determine λ^2 from the ratio of I_{in}/I, where I_{in} and I represent the inelastic component and the total tunneling current, respectively, the IETS peak height has to be spatially mapped in a constant-current STM regime.
[24] H. H. Weitering, D. R. Heslinga, and T. Hibma, Phys. Rev. B **45**, 5991 (1992).
[25] I. Altfeder, A. A. Voevodin, and A. K. Roy, Phys. Rev. Lett. **105**, 166101 (2010).
[26] I. B. Altfeder, K. A. Matveev, and D. M. Chen, Phys. Rev. Lett. **78**, 2815 (1997).
[27] P. Czoschke, H. Hong, L. Basile, and T.-C. Chiang, Phys. Rev. B **72**, 075402 (2005).
[28] A. Mans, J. H. Dil, A. R. H. F. Ettema, and H. H. Weitering, Phys. Rev. B **66**, 195410 (2002).
[29] W. B. Su, S. H. Chang, W. B. Jian, C. S. Chang, L. J. Chen, and T. T. Tsong, Phys. Rev. Lett. **86**, 5116 (2001).
[30] J. M. Rowell, W. L. McMillan, and W. L. Feldmann, Phys. Rev. **180**, 658 (1969).
[31] S. de Gironcoli, Phys. Rev. B **51**, 6773 (1995).
[32] The oscillatory portion of $\lambda(H)$ dependence, reported in Refs. [18,19], has to do with oscillations of $\Delta k = Q(H) - q$.
[33] Suppression of interference for short-wavelength QW modes is equivalent to the low-pass filtering of curve 1 in Fig. 1.
[34] The conclusions of our work are valid for the class of materials with a nearly half-filled conduction band ($2k_F \approx q$).